UNIVERSITY OF CALIFORNIA, SAN DIEGO

Experimental Validation of Flow Properties in a Novel Y-graft for the Fontan Surgery

A Thesis submitted in partial satisfaction of the requirements
for the degree Master of Science

in

Engineering Sciences (Mechanical Engineering)

by

Craig Vermeyen

Committee in charge:

Professor Alison Marsden, Chair
Professor Juan Lasheras
Professor Vishal Nigam

2010

The Thesis of Craig Vermeyen is approved and it is acceptable in quality form for publication on microfilm and electronically:

Chair

University of California, San Diego

2010

Dedication

I want to dedicate this thesis to my parents, Joann and Robb Vermeyen, who have encouraged me throughout my childhood to pursue a higher education and instilled in me the dedication and responsibility required to bring my goals to fruition.

Table of Contents

List of Figures

Acknowledgements

I would like to acknowledge Professor Alison Marsden for giving me the opportunity to be involved in this research endeavor and her guidance throughout my graduate schooling.

I would like to acknowledge Vikram Juneja, Esteban Mendoza, Michael Pattanachinda and Alice Huang, who as part of an undergraduate team worked with me to develop a first prototype of the Y-graft model, and to perform qualitative flow analysis using dye.

I would like to acknowledge Marten Coulter for his aid in the process of improving the Y-graft model, and Alice Huang again for her collaboration while refurbishing the pulsatile pump used for physiological flow simulation.

I would like to acknowledge Weiguang Yang, Dibyendu Sengupta and Sethuraman Sankaran of the Marsden research group for their work on the simulation side of this project. Their extensive knowledge and guidance in the field of computational fluid dynamics was imperative to the completion of this project.

I would like to acknowledge Chris Cassidy for the time he allowed me in the Design Studio, as well as Tom Chalfant and Dave Lischer for all of their Machine Shop guidance.

ABSTRACT OF THE THESIS

Experimental Validation of Flow Properties in a Novel Y-graft for the Fontan Surgery

by

Craig Vermeyen

Master of Science in Engineering Sciences (Mechanical Engineering)

University of California, San Diego, 2010

Professor Alison Marsden, Chair

Numerical analysis has become an increasingly popular tool in the scientific community. Specifically, computational fluid dynamics (CFD) has become a standard in the field of fluid dynamics research. Although data generated using this technique is generally accepted as being reliable, experimental validation is still highly necessary to add credibility to scientific results. This paper aims to experimentally validate numerical results obtained on the fluid dynamics of internal flow of an extracardiac Y-shaped graft used to treat children with single ventricle congenital heart disease. Through a comparison with PIV analysis, the numerical data is shown to be quite accurate despite an increased complexity of flow in the experimental data, most likely attributable to surface effects not captured in the simulations. Hence, feasibility of

performing in vitro validation of simulation data is demonstrated. In addition, a comprehensive model-building process, which results in a physiologically accurate and PIV-ready model, is presented.

Chapter 1. Introduction

Hypoplastic Left Heart Syndrome (HLHS) and Tricuspid Atresia are two examples of congenital heart disease that require a three-staged surgery to correct. HLHS is the fourth most common affliction which requires neonatal open heart surgery and is the most common cause of death by congenital heart disease in the first year [1] [2].

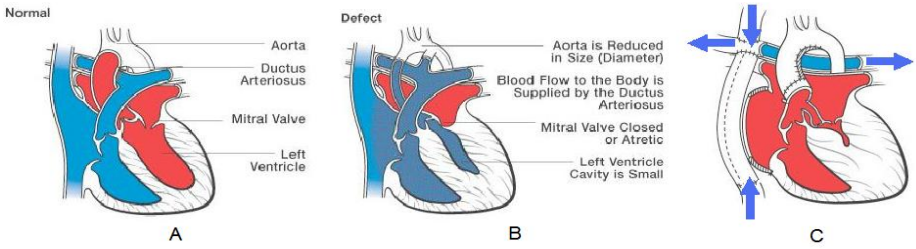

Figure 1. A) Normal heart B) HLHS heart C) HLHS heart post surgery.

Single ventricle heart patients typically undergo a three-staged surgical palliation. The end result is the conversion of the circulation from a two-pump system to a one pump system, and separation of the systemtic and pulmonary circulations. The first stage of the surgery, a Norwood procedure, is used to reconstruct the aorta and insert a shunt between the systemic and pulmonary circulations. The Glenn procedure is used next to connect the superior vena cava (SVC) directly to the pulmonary arteries (PA). The last surgery, the Fontan procedure, creates a T-Junction by attaching the inferior vena cava (IVC) to the pulmonary arteries (PA). Although this series of surgeries enables many afflicted children to live relatively normal lives (despite respiratory problems at exercise, increased incidence of arrhythmias and

thrombosis, and even heart failure) [3] there are significant improvements to be made in the efficiency and flow distribution of the arterial connection method. Marsden et al [4] have shown that a novel Y-shaped graft design can improve flow efficiency and minimize energy dissipation, leading to improved hemodynamics and cardiovascular function at exercise. This paper aims to experimentally validate the numerical results found using computational fluid dynamics by Marsden et al.

Chapter 2. Background

The Y-graft design has been compared in simulations to the original t-junction design, as well as the relatively new offset method [4]. The t-junction design attaches the IVC and SVC to the pulmonary arteries at one single point in such a way that impinging flow from the opposing venae cavae impact with significant energy loss. To correct for this, a new design was adopted which offset the venae cavae and hence alleviated the issue of energy dissipation [5]. Although the design is more efficient in this sense, other issues such as IVC flow distribution (important due to the hepatic factor contained in IVC blood that is crucial for normal lung development) and arterial pressure remained problematic. Patient specific models were developed through MRI data (at rest and exercise) to be used in the CFD analysis. Through this simulation based hemodynamic evaluation, four clinically motivated performance measures of the Y-graft were examined: Fontan pressure, energy efficiency, IVC flow distribution, and wall shear stress. It was shown that the Y-graft increased energy efficiency at both rest and exercise, and also more accurately distributed the IVC flow to the pulmonary arteries [4].

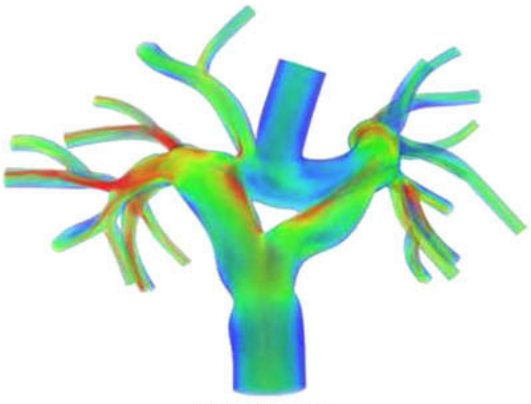

Figure 2. Idealized Y-graft design.

Now that the benefits of the Y-graft had been numerically validated, the design was optimized to maximize improvements to these parameters. For this purpose, idealized 3D models of the Y-graft Fontan geometry were created using the open-source software Simvascular.

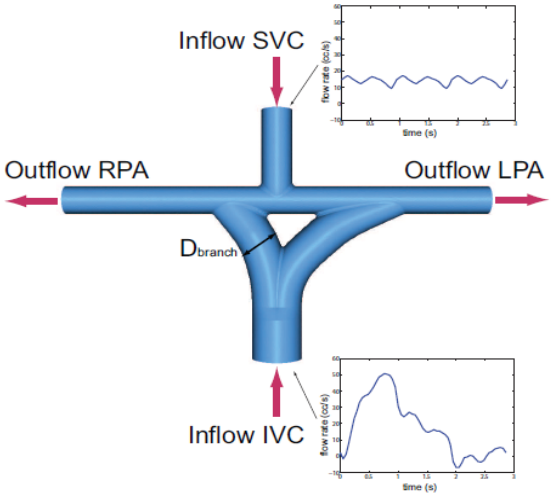

Figure 3. Simvascular model of idealized Y-graft.

The IVC, Y-graft, SVC, and PAs were defined analytically and then constructed by lofting together a series of circles and ellipses [6]. The optimization of the model was parameterized by the diameter of the Y-graft branches, length of the IVC trunk, positions where the left and right branches of the Y-graft connect to the PAs, and two final parameters which characterize the curvature of each branch of the graft. The CFD simulation was run again through Simvascular to solve the 3D Navier-Stokes equations with a finite element solver. The rigid wall and Newtonian fluid approximations were used with an assumed blood viscosity and density of 0.04 g/cms and 1.06 g/cm^3, respectively. Outlet resistance was chosen such that the IVC pressure would be 12 mm Hg, which is a reasonable clinical value. Also, the RPA/LPA flow split was set at 50/50. Similar but slightly more favorable results to the work by Marsden were found for these models.

To experimentally validate the optimized results, the physical model and flow conditions would have to be as close as possible to those in the numerical simulation. The relevancy of the results of this study relies on this fact.

Chapter 3. Model Construction

The physical model of the Y-graft was to be constructed of an optically clear material so as to facilitate the use of laser illumination of particles in the flow during PIV analysis. Initial constructions of the model were used mainly to determine the best choice of material, and best method of production. Several factors would influence the final design; namely clarity, physiological accuracy, and ease and cost of construction.

The materials selection process really only focused on two options. In order to maintain model transparency it was decided that either clear resin or silicone would be used to cast the model. Both of these materials would facilitate the lost-wax technique of casting. Lost-wax involves pouring uncured material around a wax model, and then melting away the wax (once the material is cured) to leave a perfect negative of the wax model. In this way we could create an exact negative of our model in a translucent material.

Due to the relative affordability of resin, our first attempt utilized this media. This cast was performed as more of a proof-of-concept and was completed prior to the development of a process to create a physiologically accurate wax model, as can be seen in Figure 4.

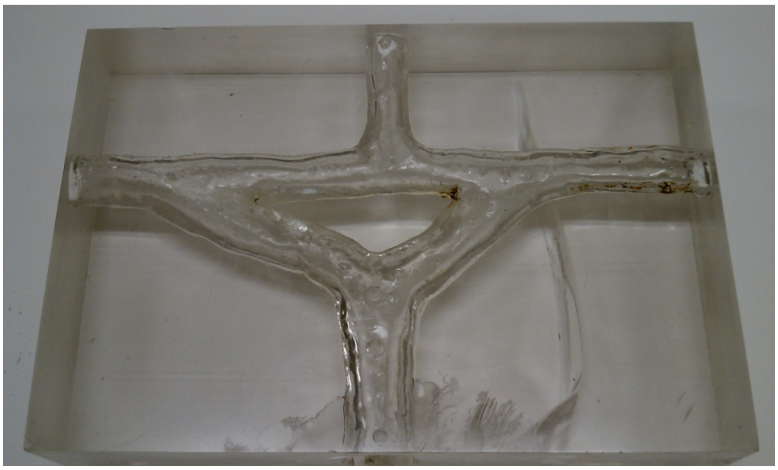

Figure 4. Preliminary model constructed using the lost-wax technique.

It is apparent then that there were several issues with this method that would not be satisfactory for our purposes. First, in order to generate useful data we would need to devise a method to recreate the exact physiology used in the numerical analysis. Secondly, a rather large blemish can be seen to mar the clarity of the resin model. This type of imperfection cannot be tolerated if Particle Image Velocimetry (PIV) analysis is to succeed (to be discussed later). It was found that the thermal energy released by the curing of the resin in fact melted the wax model prematurely, which resulted in the liquid wax snaking its way through the semi-cured resin, and ruining the clarity. Also, less importantly for our purposes, the hardness of resin allows no flex in pulsatile flow, which is present in arteries in actual hemodynamic flows. For all of these reasons it was decided that silicone would provide a more desirable casting material.

First it was necessary to develop a process for creating an accurate wax model of the solid model used in the computational analysis. The ideal would have been to

print an exact model in wax or water-soluble material using a 3D printer, however, the printer available to us could not print in either of these materials. It could, however, print in ABS plastic.

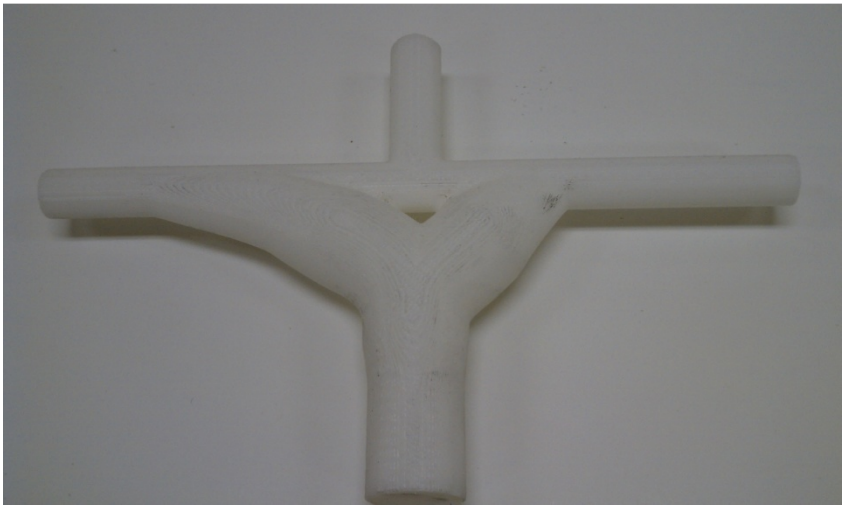

Figure 5. ABS plastic model printed using 3D printer.

To obtain a wax model from this ABS model it was decided to make a two-part negative mold of the ABS model using the resin molding material. From here the two halves could be separated and the ABS printed model removed. Next, the resin negative was filled with liquid wax and allowed to cool. Once the wax had hardened again, the two halves of the mold were separated to reveal the exact wax replica of the original ABS print.

Figure 6. Resin model with wax model inside.

The next decision involved determining the best method for creating the silicone mold from this wax model. Ideally, a thin-walled model closely resembling actual arterial physiology would have been constructed in the method of Ryan Wicker et Al. [7] at the University of Texas at El Paso. Unfortunately, their complex process requires a sizable fee, which we were unable to provide. Significant time was invested in a feasibility study of their method to determine if we could build the necessary apparatuses to perform the model construction ourselves.

Professor Wicker named his thin-walled silicone model construction method the “Dip-Spin Method” because the wax (or water soluble) model is repeatedly dipped in silicone and then spun on multiple axes to ensure even coverage. In this way, each layer of silicone builds on the next and begins to cure and meld with the surrounding layers. Once the desired thickness is achieved, the entire model is allowed to cure for a few days before the wax is melted to leave the hollow thin-walled vessel. The dipping apparatus consists of a stepper motor attached to a frame that lowers and

raises the model into a container of silicone at a pre-programmed speed (a function of viscosity, which can be varied through the addition of xylene) to most effectively coat the model.

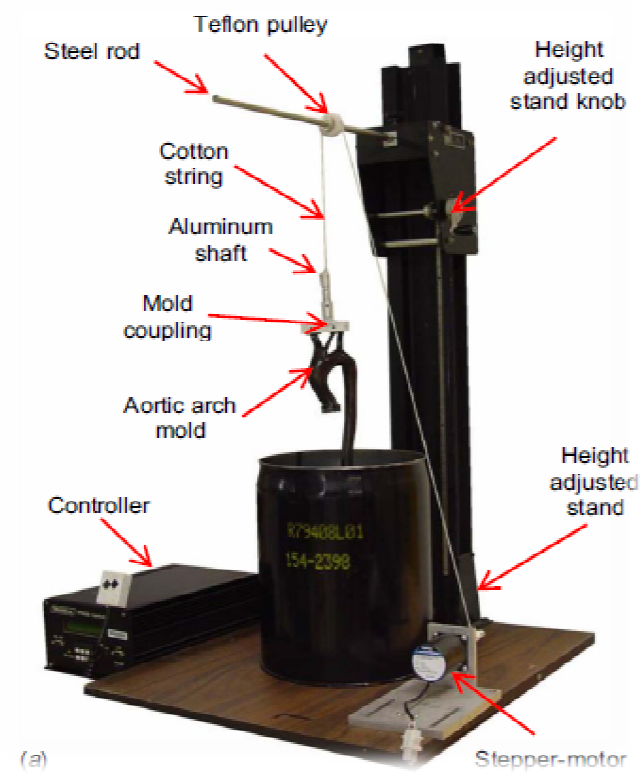

Figure 7. Dr. Ryan Wicker's dipping mechanism.

The model is then transferred to a spinning mechanism that consists of two motors that spin in perpendicular planes to evenly distribute the silicone on the surface of the model.

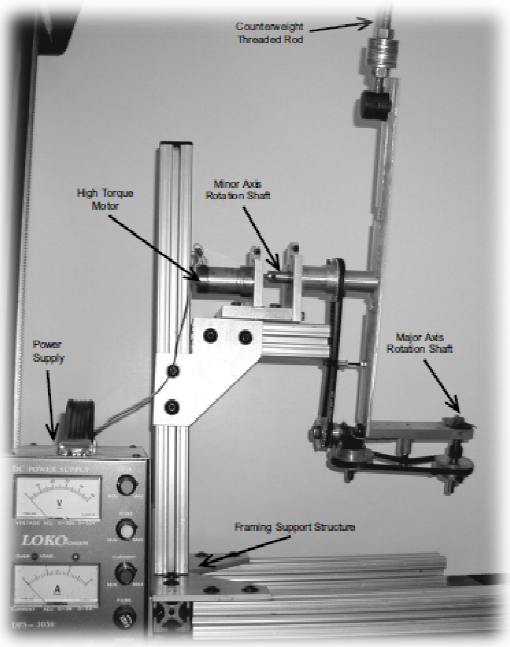

Figure 8. Dr. Ryan Wicker's spinning mechanism.

These steps are then repeated as desired. It was determined that it would be possible to design and manufacture our own dipping and spinning apparatuses, but at a cost of significant time and effort. It was then decided that an alternative method could be used to build the model much more quickly without sacrificing much (if any) credibility of results.

This alternate method involves casting the wax model in a solid block of silicone, which negates the need for the construction of any complex mechanisms, and simply requires the construction of a box to perform the casting in. This was the method used in the initial proof-of-concept resin model construction. It is slightly less desirable than the thin-walled method for two reasons. Most importantly, PIV analysis hinges on the ability of laser light to penetrate the model and illuminate

reflective particles in the flow. The more material the laser must penetrate, the more opportunities for imperfections in the material to diminish the strength of the laser and cast shadows in the flow geometry. However, with careful casting techniques and some clever positioning in the apparatus, these issues can for the most part be avoided. Another minor issue is the decreased physiological accuracy encountered in block-modeling. Arterial wall flexing cannot be as closely mimicked when the walls are approximated as a block; though the inherent ductility of silicone does allow some give during pulsatile flow.

The block modeling process begins with the construction of an appropriately sized box. The box will be used to suspend the model in silicone for casting, and must incorporate enough extra room along each edge for the addition of Tygon fittings (connectors used to attach tubing between the pump and the model). Acrylic was chosen for the design of the box because of its availability, and its ability to be cut using UCSD's LaserCAMM laser cutting tool. The machine is supplied with an AutoCAD file of the shape to be cut, and it uses a focused laser to slice through the acrylic with precision and speed. In this way some specially formulated acrylic glue (covalent bonding) and silicone sealant are all that is required to create a liquid-tight container for casting.

Before casting it was necessary to treat the surface of the wax model for two important reasons. First, small surface imperfections resulted from the multi-step molding process, and a high-build surface primer (UPol High #5) was used to fill in and smooth these chips and grooves. It was also necessary to completely encapsulate

the wax model in a liquid tight coating so as to avoid fogging of the silicone model as the wax was melted away. Though the primer also worked to this end quite well, it was found through numerous trials that a layer of glue (Elmer's School Glue) helped seal an gaps in the primer as well as facilitate removal of the primer once the wax had been removed.

The model was then suspended in the box by way of screwing the Tygon fittings through a hole on each of the four walls of the box so that once the silicone had cured these would create the connection points for the tubing.

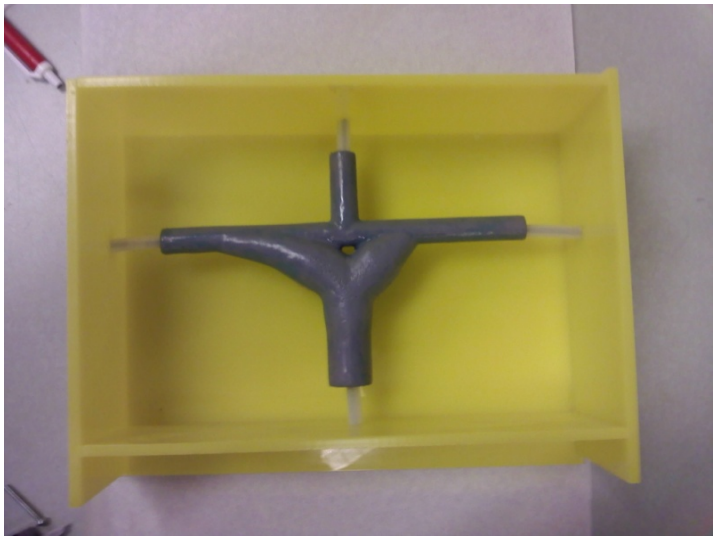

Figure 9. Model coated in primer and glue and suspended in acrylic box.

Silicone (Dow Corning Sylgard 184) was mixed (10:1 silicone to curing agent by volume) and degassed at 15 atmospheres in a National degassing oven. The uncured silicone was then slowly and carefully poured into the box containing the cast until the model was completely covered by approximately 2 centimeters of silicone.

This was then left to cure for almost four days to ensure the entire volume was completely hardened before removal from the box.

The edges of the box were then peeled away to ready the model for wax-removal.

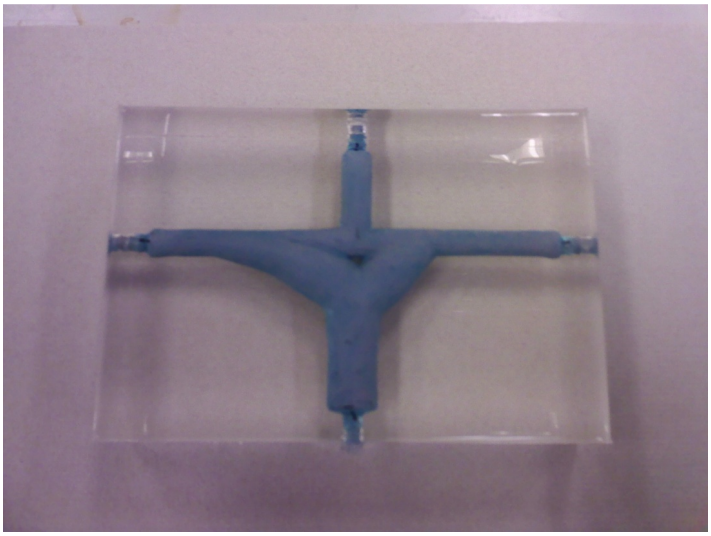

Figure 10. Silicone model prepared for wax-removal.

A standard kitchen oven set to 300 □ F was used to heat the wax to its melting point so it would run easily out of the silicone model. Great care was taken to route the melting wax away from the sides of the model to avoid clouding of these surfaces. The primer and glue was removed using a medium stiff bristle pipe cleaner and a flexible claw grabber pick-up tool. The interior surfaces of the flow passageways were then cleaned using cotton swaps soaked in acetone to ensure the best clarity possible. To facilitate connection to the pumping apparatus, male Tygon tube fittings were glued into each inlet and exit of the model, and sealed with silicone sealant.

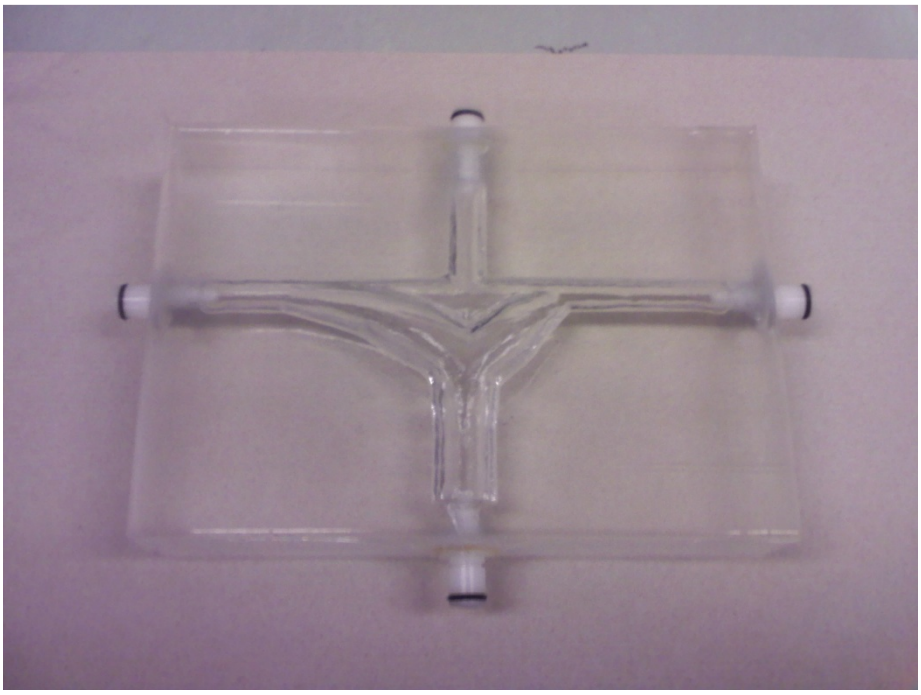

Figure 11. Completed silicone model including tubing fittings.

Chapter 4. The Testing Apparatus

A UHDC pulsatile flow pump was used to simulate hemodynamic conditions in the model. The pump was filled with a blood-simulating fluid (60% water 40% glycol) which contained tiny particles of Lycopodium which would be used to trace streaklines in the flow. The pump consists of a piston/cylinder assembly that can be programmed to simulate any wave form required. In this way actual blood flow patterns in different areas of the body can be replicated. Tygon tubing is run from the pump output and split into two to supply flow to the IVC and SVC inputs of the model. Two tubes then exit each pulmonary artery output from the model, and are combined into a single tube to be fed back into the pump. The model is placed on an optical table in front of a YAG laser (TSI) which will be used to illuminate particles in the flow. A CCD camera is placed on a tripod above the model to record images of the particles in the flow.

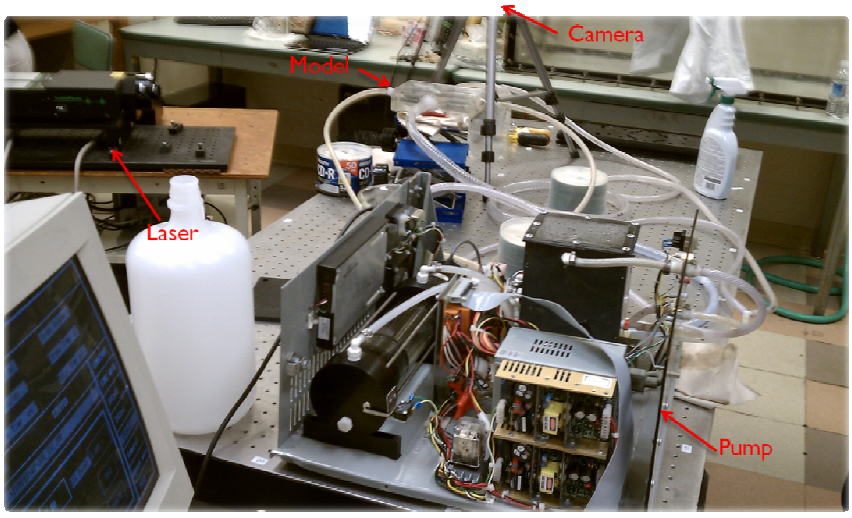

Figure 12. Experimental setup.

This camera is connected to a computer, which uses Insight 3G software to analyze the images and return velocity data at each point in the laser plane. This software takes tandem images at a pre-determined interval and analyzes the change in position of the particles to determine the flow velocity. The resulting data can then be used to determine flow properties throughout the model.

Chapter 5. PIV Testing Procedure

To begin, the concentration of Lycopodium particles in the water/glycol mix is verified to ensure there are enough particles that the software can reliably determine flow in all areas, and that there are not too many particles that the software becomes confused. This is done by placing a beaker of the final mix in front of the laser and visually verifying the number of particles. Next, the laser is aligned with the model in such a way that laser plane passes through the center plane of the model. In this way, the velocities through the center plane of the model can be visualized and recorded. The CCD camera records 100 pairs of at 14.5 frames per second. The images are saved on a computer (Intel Core2 8400) for processing by the Insight 3G software.

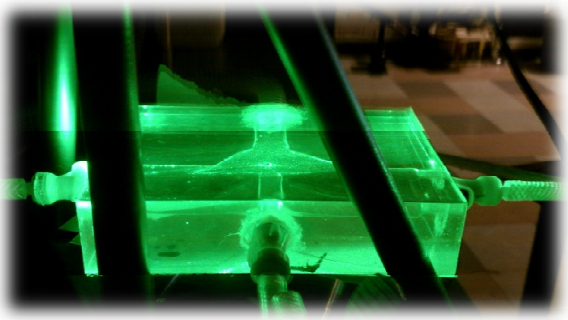

Figure 13. Model illuminated by laser light while capturing images.

Image processing begins with the application of a mask to the set of images to specify which areas are to be analyzed. Next, a post-processing routine is built to clean-up the velocity data that is returned by the software. Three stages of post-processing are performed to improve the quality of results:

- First, Global Validation is performed to remove all errant vectors with values above three standard deviations different than the mean velocity.
- Next, Local Validation is used to replace a vector that is above or below a threshold of the median of each vector immediately surrounding it, with the median value itself.
- Lastly, Vector Conditioning fills holes in the data with the local median, and smoothes the data by replacing each vector with its Gaussian weighted mean of the neighbor vectors.

Finally, the analysis is run and the software returns vector fields on each image, and velocity magnitudes at each spatial location.

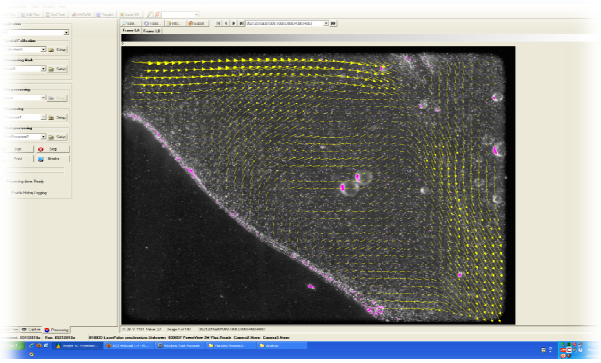

Figure 14. Example vector field in a portion of the model.

Chapter 6. Results

The experimental data that were produced in the PIV analysis were compared to the data produced by the simulation. First, a qualitative comparison of the two data was performed at points in the cardiac cycle, which correspond to the average, minimum and maximum flow rates. As can be seen in Figure 15, the LPA section of the Y-graft shows significantly more complexities in the experimental flow.

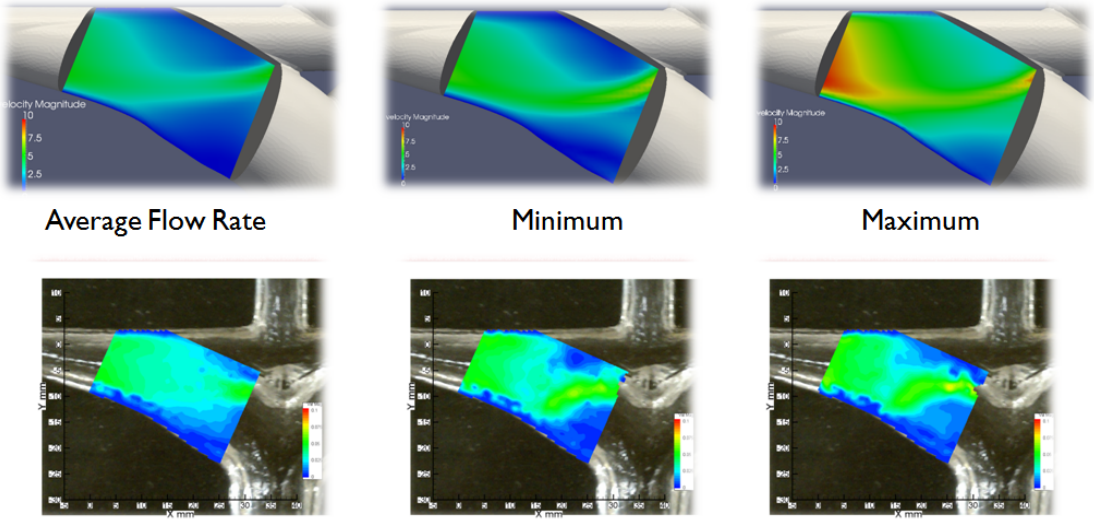

Figure 15. Qualitative comparison of LPA simulation and experimental velocity distributions.

Similarly, the experimental flow in the RPA section of the Y-graft appears to involve much more turbulence and mixing.

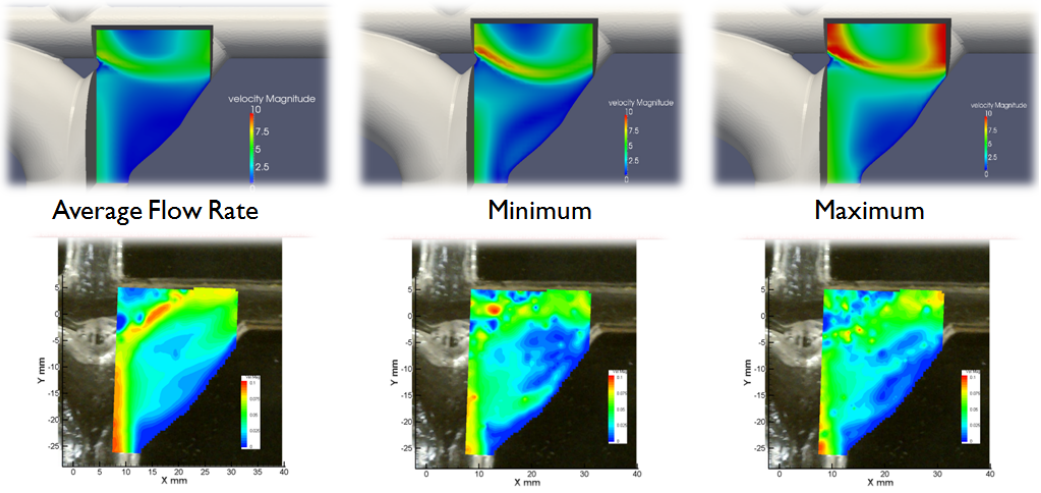

Figure 16. Qualitative comparison of RPA simulation and experimental velocity distributions.

Next, time averaged velocity profiles in both the LPA and RPA sections of the Y-graft were measured to compare to the simulation profiles.

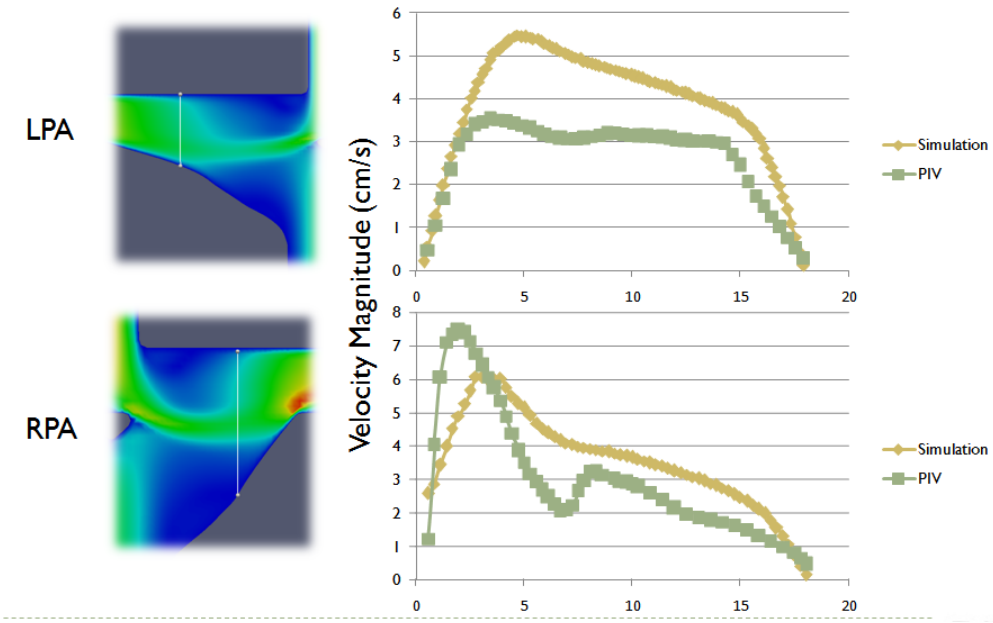

Figure 17. Time averaged velocity profiles across the LPA and RPA branches.

Also, the wall shear stress (WSS) that acts on the arterial walls over the course of the cycle is important for determining the risk of thrombus formation. To determine if the simulation correctly predicted improvements in this area, Tecplot software was used to create the shear stress distribution from the experimental data. As Figure 18 shows, the values along the wall in the experimental data are very similar to those predicted on the wall of the simulation model.

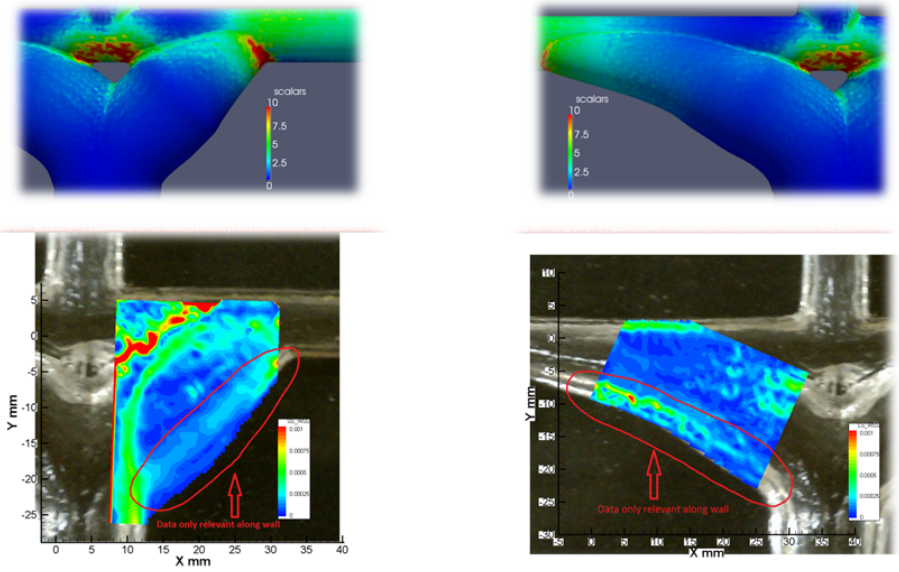

Figure 18. Qualitative depiction of shear stress in the simulation and experiment.

From a qualitative comparison of the experimental and simulation velocity magnitude videos, it was thought that the vorticity would be an interesting distribution to see. Figure 19 depicts the differences between the simulation and experimental vorticity.

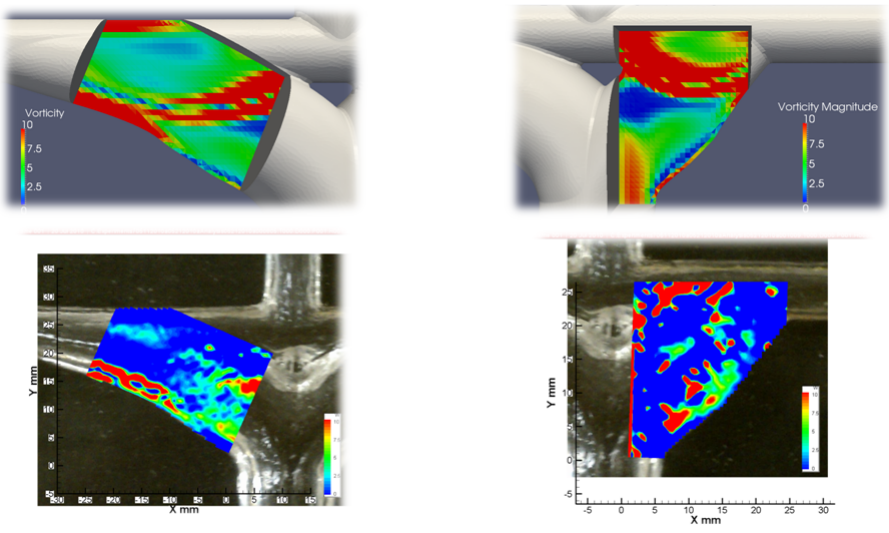

Figure 19. Qualitative depiction of vorticity in the simulation and experiment.

Chapter 7. Discussion

The most obvious difference between the simulation and experimental results is the increased complexity of the flow in the experimental data. It is thought that this is predominantly due to surface effects, which are not taken into consideration in the simulation. Smooth rigid walls produce much cleaner flow distributions than physiological conditions. The slight give in the walls of the silicone model are closer to actual arterial tolerance. Wall flexing during the cardiac cycle may lead to the flapping turbulent flow we can see most pronounced in the LPA section of the Y-graft.

The images comparing velocity magnitude distributions in the simulation and experimental data reveal that the velocities are very similar, though flow speeds in the simulation seem to be slightly higher. The increased friction at the walls of the experimental model may contribute to this slight decrease in velocity from the simulation data.

The comparison of velocity profiles across each branch of the Y-graft also shows that the velocities are slightly lower in the experimental data. The profiles do however match quite well, with differences most likely attributed to the inability to accurately characterize the IVC/SVC flow distribution in our experimental setup. It can be seen in Figure 16 that there appears to be significantly more flow from the IVC in the experiment.

Due to the increased complexity of the flow in the experiment it was thought that WSS values would be higher. Figure 18 confirms that this is in fact the case.

WSS is a function of the velocity gradient along the wall, which is higher in the experimental case due to the areas of recirculation.

These areas of recirculation should also result in increased vorticity in the experimental data, but Figure 19 shows that these areas of higher vorticity are confined to much smaller areas of the flow. The flapping nature of the more turbulent experimental flow causes small eddies of high vorticity to propagate through the branches of the Y-graft..

Chapter 8. Conclusions

Overall it can be seen that flow is much more complex throughout the Y-graft in the experimental data. Surface effects not captured in the computational model result in turbulent flapping flow in the branches of the graft.

However, the similarity of velocity magnitudes and profiles in the graft found computationally and experimentally lend credibility to the computational analysis, and to the improved fluid characteristics of the graft measured in this model. Through this work we were able to demonstrate the feasibility of performing in vitro validation of simulation data.

Perhaps equally importantly, a method of construction for a PIV phantom model was developed and improved such that it can be completed in approximately one week's time. Though this method is only useful for geometries that are symmetric about one plane, it is comprehensive and consistently returns quality models which fit the criteria for PIV analysis: optical clarity, wall smoothness, and appropriate index of refraction.

Chapter 9. Sources of Error/Limitations

There were several sources of error through the course of this study that limit its applicability to physiological conditions. First, and perhaps most troubling, the waveform used to simulate cardiac output in our pump was significantly altered to fit the capabilities of the pump. Both the peak and mean flow rates were required to be decreased so as to not overwork the pump. This has clear implications on applicability of flow patterns in the simulation matching in vivo results.

Also, the experimental setup introduced significant inaccuracy with regards to flow rate and flow distribution in addition to highly approximated inlet and outlet conditions. The numerous orifices used to connect the tubing lengths and the model introduced unmeasured pressure gradients which surely affected IVC/SVC flow distribution (see Figure 16). Hemodynamic impedance matching was outside the scope of this study, and hence outflow conditions in the experiment may differ greatly from reality.

Though smaller in scale than those previously mentioned, the inherent difficulties with the model building process added still more faults to the experimental results. Despite great care having been taken to ensure smooth interior passage walls, tiny imperfections were still apparent. In addition, slightly oversized passage diameters may have resulted from the primer and glue steps of the process.

Another minor source of error worth mentioning is the discrepancy in fluid characteristics between our experimental working fluid and blood. Although an attempt at matching viscosities was made, the glycol/water mix behaves as a

Newtonian fluid – while blood does not. This seemingly insignificant fact may drastically change complex fluid dynamics.

Similarly, the silicone model does provide some elasticity in the passageways (visible flexing of the model was apparent while experiencing pulsatile flow); however no attempt was made to match the elasticity of arterial walls. The complex internal flows in our experiment surely would show a change if the wall elasticity was altered.

Finally, it was thought that perhaps the PIV analysis was not performed at the centerline of the model as was done in the simulation and this would result in different flow patterns. A thorough study of simulation profiles was conducted at one, two and three millimeters from the centerline of the simulated model in both directions to facilitate observation of changes this might have on the profile. Figure 20 clearly shows that very little change occurs and thus this was most likely not a significant source of error.

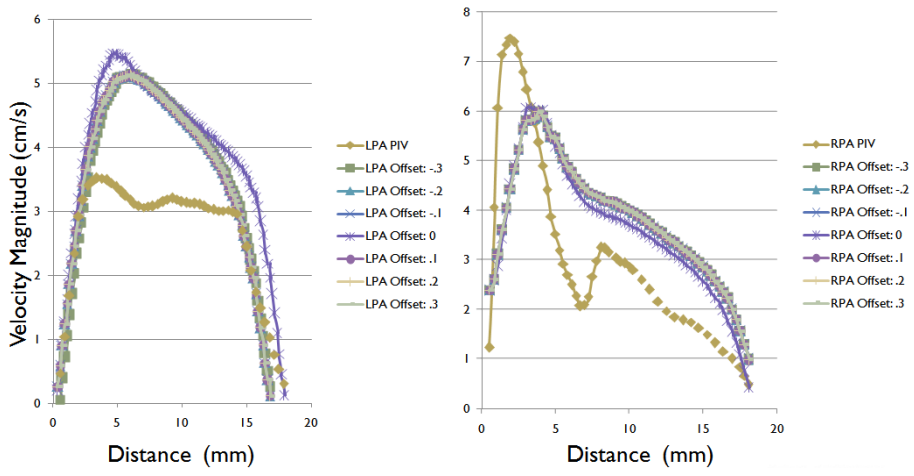

Figure 20. Offset profiles showing little change.

Chapter 10. Future Work

As seen above, this is just the beginning of this work. There are several areas for significant improvement, which will help to yield more applicable and publishable results.

First, improving the optical clarity and smoothness of the model is imperative. It may even be worthwhile to invest in mechanisms to facilitate the use of Dr. Wickers Dip-Spin method eventually. My colleague Alice Huang and I were already able to improve the optical clarity of a block model for a project she has been working on.

Also, improvement to the inlet and especially outlet boundary conditions may yield much more accurate results. Several papers have cited the use of a mechanical RCR circuit [8] to more accurately model downstream impedance.

A simply and effective way to increase the reliability of these results would be too obtain a new pump or modify the existing pump to handle the actual physiological cardiac waveform. This would make it much easier and clearer to compare to patient data to more thoroughly validate the computational findings.

Finally, much time could be well spent determining a more effective and reliable way to determine wall shear stress from the PIV data for comparison with computational data. This experiment was only able to show limited data from a single slice through the center plane. This provides very few data points on the physical surface of the model. A 3D PIV technique may be used in the future to facilitate analysis of shear stress along the entire surface of the silicone model, thus making comparison to the computational model much more enlightening.

Appendix

Waveform Data Points Used in Pulsatile Pump

t_space'	pumpin	modIVC	modSVC
0	13.3140	7.9884	5.3256
0.0282	12.3337	7.4002	4.9335
0.0564	11.3534	6.8120	4.5414
0.0846	12.2639	7.3584	4.9056
0.1128	13.1745	7.9047	5.2698
0.1410	14.2700	8.5620	5.7080
0.1692	15.3655	9.2193	6.1462
0.1974	17.9101	10.7460	7.1640
0.2256	20.4546	12.2727	8.1818
0.2538	22.7273	13.6364	9.0909
0.2821	25.0000	15.0000	10.0000
0.3103	24.7981	14.8789	9.9192
0.3385	24.5962	14.7577	9.8385
0.3667	23.9371	14.3622	9.5748
0.3949	23.2779	13.9667	9.3112
0.4231	22.7820	13.6692	9.1128
0.4513	22.2860	13.3716	8.9144
0.4795	21.2507	12.7504	8.5003
0.5077	20.2155	12.1293	8.0862

0.5359	18.7999	11.2799	7.5199
0.5641	17.3842	10.4305	6.9537
0.5923	17.0167	10.2100	6.8067
0.6205	16.6491	9.9894	6.6596
0.6487	16.3860	9.8316	6.5544
0.6769	16.1230	9.6738	6.4492
0.7051	16.3004	9.7802	6.5201
0.7333	16.4777	9.8866	6.5911
0.7615	16.8696	10.1217	6.7478
0.7897	17.2614	10.3568	6.9045
0.8179	17.7327	10.6396	7.0931
0.8462	18.2040	10.9224	7.2816
0.8744	18.6246	11.1748	7.4499
0.9026	19.0452	11.4271	7.6181
0.9308	18.3929	11.0357	7.3572
0.9590	17.7406	10.6443	7.0962
0.9872	17.4639	10.4783	6.9856
1.0154	17.1872	10.3123	6.8749
1.0436	16.3139	9.7883	6.5256
1.0718	15.4405	9.2643	6.1762
1.1000	14.3773	8.6264	5.7509

Bibliography

[1] R.F. Gillum. *Epidemiology of congenital heart disease in the United States.* Am Heart J, 1994

[2] D.C. Fyler. *Report of the New England Regional Infant Cardiac Program*. Pediatrics, 1980

[3] A. Marsden. *Effects of Exercise and Respiration on Hemodynamic Efficiency in CFD Simulations of the Total Cavopulmonary Connection*, Ann Biomed Eng, 2007

[4] A. Marsden. *Evaluation of a novel Y-shaped extracardiac Fontan baffle using computational fluid dynamics*, J Thorac Cardiovasc Surg, 2009

[5] A.P. Yoganathan. *Toward Designing the Optimal Total Cavopulmonary Connection: An In Vitro Study*, Ann Thorac Surg, 1999

[6] W. Yang. *Constrained optimization of an idealized Y-shaped baffle for the Fontan surgery at rest and exercise*, Dissertation, 2009

[7] R. Wicker. *Patient-Specific Compliant Vessel Manufacturing Using Dip-Spin Coating of Rapid Prototyped Molds*, Journal of Manufacturing Science and Engineering, 2008

[8] E. Kung. *In Vitro Validation Of Finite Element Model Of AAA Hemodynamics Incorporating Realistic Outflow Boundary Conditions*, Proceedings of the ASME 2010 Summer Bioengineering Conference, 2010

[9] W. Yang, J.A. Feinstein, A.L. Marsden. *Constrained Optimization of an idealized Y-shaped baffle for the Fontan surgery at rest and exercise*, Computer Methods in Applied Mechanics and Engineering, 2010

[10] A.L. Marsden, I.E. Vignon-Clementel, F.Chan, J.A. Feinstein, C.A. Taylor. *Effects of exercise and respiration on hemodynamic efficiency in CFD simulations of the total cavopulmonary connection*, Annals of Biomedical Engineering, 2007

[11] A.L. Marsden, V.M. Reddy, S.C. Shadden, F.P. Chan, C.A. Taylor, J.A.Feinstein. *A new multi-parameter approach to computational simulation for Fontan assessment and redesign*, Congenital Heart Disease, 2010

[12] Y. Bazilevs, M.C. Hsu, D.J. Benson, S. Sankaran, A.L. Marsden. *Computational Fluid-Structure Interaction: Methods and Application to a Total Cavopulmonary Connection*, Computational Mechanics, 2009

[13] A. Sulaiman. *In Vitro, Nonrigid Model of Aortic Arch Aneurysm*, J Vasc Interv Radiol, 2008

[14] C.K. Chung. *Flow Visualization in a Model of a Bifurcated Stent-Graft*, J Endovasc Ther, 2005